Supporting Information

Amorphous FeOOH-modified spongy steamed-twisted-roll SnS_2/Ni_3S_2 hierarchical electrocatalyst for efficient oxygen evolution reaction

Shi-Jing Wang,[a,1] Xing Liu[a,1], Xiao-Yan Chen and Jian Zhou[a,*]

[a]*Chongqing Key Laboratory of inorganic functional materials, College of chemistry, Chongqing normal university, Chongqing, 401331, P.R. China*

Corresponding author:

Prof. & Dr. Jian Zhou

****

Prof. & Dr. Jian Zhou

College of chemistry,

Chongqing normal university

Chongqing, 401331,
P.R. China
E−mail: Jianzhou888888@163.com
****

[1]These authors contributed equally.

S1 Experimental section

S1.1. Materials

Ruthenium(II) oxide (RuO_2, more than 99.9% pure), platinum on carbon (Pt/C, 20% by weight), thioacetamide (C_2H_5NS, at least 99% pure), and tin(IV) chloride pentahydrate ($SnCl_4·5H_2O$, at least 99% pure) were obtained from Shanghai Macklin Biochemical Technology Co. Ltd. Hexahydrated nickel(II) nitrate ($Ni(NO_3)_2·6\ H_2O$, more than 98% pure), potassium hydroxide (KOH, at least 90% pure), and ethanol (C_2H_6O, at least 99 Hexahydrated nickel(II) nitrate ($Ni(NO_3)_2·6\ H_2O$, purity ≥ 98%), potassium hydroxide (KOH, purity ≥ 90%), and ethanol (C_2H_6O, purity ≥ 99.7%) were supplied by Chengdu Kolong Chemical Reagent Factory. Urea ($CO(NH_2)_2$, purity ≥ 99%) was acquired from Sinopharm Group Chemical Reagent Co. Ltd. Ammonium fluoride (NH_4F, purity ≥ 96%) was acquired from Shanghai Aladdin Biochemical Technology Co., Ltd. Hydrochloric acid (HCl, purity ≥ 36%) and acetone (C_3H_6O, purity ≥ 99.5%) were procured from Chongqing Chuandong Chemical Co.Ltd. Graphite rods (≥ 99.995%, diameter 6 mm) were procured from Shanghai Yuema Electronic Technology Co., Ltd. by Suzhou Sainteno Technology Co., Ltd. Hg/HgO (1 mol·L^{-1} KOH) was acquired from Tianjin Aida Technology Development Co., Ltd., and the 1.6 mm thick nickel foam (NF) was sourced from Kunshan Yunzongcheng Materials Co.Ltd.

S1.2. Preparation of nickel precursors with four different morphologies

Nickel-based precursors were grown on NF substrates via a hydrothermal method. The commercial NF substrate (2 cm × 3 cm) was first ultrasonically cleaned in 3 mol L^{-1} HCl solution for 15 minutes (frequency: 40 kHz) to remove the surface oxide layer. It was subsequently washed with acetone, ethanol, and DI water sequentially, and finally dried under vacuum at 60 °C for 6

hours.

S1.2.1. Preparation of nickel precursor with rose-like arrays morphology

1.5 mmol $Ni(NO_3)_2 \cdot 6H_2O$ and 5 mmol $CO(NH_2)_2$ were weighed and dissolved in 15 mL of deionized water. The mixed solution was magnetically stirred at room temperature for 30 min to obtain a clear, light green homogeneous solution. The resulting solution was transferred into a 25 mL PTFE-lined stainless steel autoclave, and a piece of pre-cleaned nickel foam (NF) was vertically immersed into the solution, followed by hydrothermal treatment at 120 °C for 6 hours. After the reaction, the green precursor product was collected, thoroughly washed with deionized water and ethanol, and then dried in a vacuum oven at 60 °C for 6 hours to obtain the nickel precursor with rose-like arrays morphology.

S1.2.2. Preparation of nickel precursor with cauliflower morphology

1.5 mmol $Ni(NO_3)_2 \cdot 6H_2O$ and 5 mmol $CO(NH_2)_2$ were weighed and dissolved in 15 mL of deionized water. The mixed solution was magnetically stirred at room temperature for 30 min to obtain a clear, light green homogeneous solution. The resulting solution was transferred into a 25 mL Teflon-lined stainless steel autoclave, and a piece of pre-cleaned nickel foam (NF) was vertically immersed into the solution. To investigate the effect of hydrothermal duration on the morphology of the nickel precursor, the hydrothermal reaction was carried out at 120 °C for 8 hours. After the reaction, the green precursor product was collected, thoroughly washed with deionized water and ethanol, and then dried in a vacuum oven at 60 °C for 6 hours to obtain the nickel precursor with cauliflower morphology.

S1.2.3. Preparation of nickel precursor with spherical morphology

1.5 mmol of $Ni(NO_3)_2 \cdot 6H_2O$ and 5 mmol of $CO(NH_2)_2$ were weighed and dissolved in 15 mL of

deionized water. The mixed solution was magnetically stirred at room temperature for 30 min to obtain a clear, light green homogeneous solution. Given that ammonium fluoride NH_4F is a commonly used morphology-directing agent in material synthesis, 2 mmol of NH_4F was added to the above solution, followed by continuous stirring until complete dissolution. The resulting solution was transferred into a 25 mL PTFE-lined stainless steel autoclave, and a piece of pre-cleaned nickel foam (NF) was vertically immersed into the solution, with the hydrothermal reaction maintained at 120 °C for 8 hours. After the reaction, the green precursor product was collected, thoroughly washed with deionized water and ethanol, and then dried in a vacuum oven at 60 °C for 6 hours to prepare the nickel precursor with spherical morphology.

S1.2.4. Preparation of nickel precursor with spongy steamed-twisted-roll morphology

1.5 mmol of $Ni(NO_3)_2 \cdot 6H_2O$, 5 mmol of $CO(NH_2)_2$ and 2 mmol of NH_4F were weighed and dissolved in 15 mL of deionized water. The mixed solution was magnetically stirred at room temperature for 30 min to obtain a clear, light green homogeneous solution. The resulting solution was transferred into a 25 mL PTFE-lined stainless steel autoclave, and a piece of pre-cleaned nickel foam (NF) was vertically immersed into the solution. The hydrothermal reaction temperature was increased to 160 °C while the reaction duration was maintained at 8 hours. After the reaction, the green precursor product was collected, thoroughly washed with deionized water and ethanol, and then dried in a vacuum oven at 60 °C for 6 hours to obtain the target nickel precursor with spongy steamed-twisted-roll morphology.

S1.3. Preparation of SnS_2/Ni_3S_2/NF with four different morphologies

The four different morphologies of Ni precursors were converted into the corresponding SnS_2/Ni_3S_2/NF via secondary hydrothermal sulfidation. Briefly, 0.5 mmol of $SnCl_4 \cdot 5H_2O$ and 3

mmol of thioacetamide (C_2H_5NS) were added to 15 mL of DI water and stirred to form a colorless transparent solution. This solution, along with the prepared Ni-precursor, was transferred into a 25 mL Teflon-lined stainless-steel autoclave. The autoclave was heated at 180 °C for 6 hours and then allowed to cool naturally to room temperature. The different morphological Ni precursors and Sn^{4+} ion are reacted with thioacetamide under hydrothermal conditions, forming the SnS_2/Ni_3S_2 heterostructures. There was no change in their morphologies when the color is changed from green to black. The products were washed several times with ethanol and DI water, and dried at 60°C. Ni_3S_2/NF was synthesized using the same hydrothermal method, but without the addition of $SnCl_4 \cdot 5H_2O$. Similarly, SnS_2 was also prepared using the same hydrothermal method, but without the NF substrate.

S1.4. Preparation of FeOOH/SnS_2/Ni_3S_2/NF with four different morphologies

The preparation of FeOOH was carried out through a simple room-temperature wet chemical process. In a typical procedure, 1 g of $FeSO_4 \cdot 7H_2O$ was dissolved in 20 mL of deionized water and stirred magnetically for 10 minutes to obtain a clear, light green solution with a concentration of 0.18 M. Subsequently, the as-prepared SnS_2/Ni_3S_2/NF sample was completely immersed in the above solution for 5 minutes. A yellowish-brown FeOOH layer gradually formed on the surface due to the oxidation of adsorbed Fe^{2+} ions. The sample was then dried in a vacuum oven at 60°C for 6 hours. Four different morphologies of FeOOH-modified hetero-structural SnS_2/Ni_3S_2 were obtained, including rose, cauliflower, spherical and spongy steamed-twisted-roll nano-arrays. For comparison, FeOOH/NF was also prepared under identical conditions by using bare NF instead of SnS_2/Ni_3S_2/NF as the substrate. Furthermore, to identify the optimal concentration for FeOOH deposition, a series of experiments were conducted with different initial concentrations of

$FeSO_4 \cdot 7H_2O$ (0.2 M, 0.18 M, 0.14 M, and 0.08 M) while keeping the immersion time constant.

S1.5. Preparation of Pt/C/NF and RuO_2 /NF electrodes

Commercial Pt/C (20 wt%) and RuO_2 were applied in combination with porous NF to fabricate Pt/C/NF and RuO_2/NF electrodes as efficient HER and OER electrocatalysts, respectively. 5 mg of catalyst (Pt/C or RuO_2) was dispersed into a mixed solution ethanol (480 μL) and 5% Nafion (20 μL), and then sonicated for 30 minutes to obtain a well-dispersed ink solution. 100 μL of the ink solution was drop-coated onto the surface of NF (1 × 0.5 cm^2) with a catalyst loading of about 2 $mg \cdot cm^{-2}$ for Pt/C or RuO_2 to achieve Pt/C/NF and RuO_2/NF electrodes.

S1.6. Physical Characterization

X-ray diffraction (XRD) patterns were acquired using a Shimadzu LAB XRD-6100 diffractometer (Cu Kα, Japan) in the range of 10 ~ 80°. The catalyst surface's chemical condition was ascertained using X-ray photoelectron spectroscopy (XPS, Thermo Scientific K-Alpha). The surface morphology of each catalyst was analyzed using field emission scanning electron microscopy (FE-SEM, SU8020, Japan) and transmission electron microscopy (TEM, JEOL JEM F200 Japan). The lattice structure and elemental composition of the catalysts were examined using high-resolution transmission electron microscopy (HRTEM) and energy dispersive X-ray spectroscopy (EDS) via field emission scanning electron microscopy, respectively. Raman spectra of the catalysts were acquired using a Raman microspectrometer (LabRAM HR Evolution, Horiba-Jobin-Yvon) with a 532 nm excitation laser. The concentrations of metal ions (Sn, Ni, and Fe) after stability testing were analyzed using an Agilent 5900 inductively coupled plasma optical emission spectrometer (ICP-OES). In-situ Raman tests were conducted on a fiber-optic confocal Raman spectroscopy system (DEEP-INRS-II, China, 523 nm laser, the laser power was 10 mW, and the

resolution was 5 cm^{-1}.) and controlled by a DH7001D electrochemical workstation at different potentials. The in situ DEMS measurements were performed using a customized setup centered on a PFEIFFER QAS 100 quadrupole mass spectrometer.

S1.7. Electrochemical measurements

The electrochemical tests in this study used a CHI 760e electrochemical workstation with a standard three-electrode setup, which had a graphite rod as the counter electrode and a Hg/HgO electrode as the reference electrode. The working electrode, with an immersion area of 0.5 cm^2, was submerged in a 1 M KOH solution, exhibiting a pH of 14, at room temperature. All potentials were adjusted to values corresponding to the reversible hydrogen electrode (RHE), utilizing the Nernst equation expressed as $E_{(RHE)} = E_{(Hg/HgO)} + 0.059\ pH + 0.098$. Each working electrode was activated several times using cyclic voltammetry (CV) tests at a speed of 20 mV per second before the linear sweep voltammetry (LSV) tests. Linear sweep voltammograms (LSV) for the oxygen evolution reaction (OER) were recorded between 1 to 1.8 V versus RHE at a scan rate of 5 $mV \cdot s^{-1}$ for all LSV profiles. All polarization curves were corrected for 90% iR compensation. Electrochemical impedance spectroscopy (EIS) measurements were conducted between the frequency range of 10^5 Hz to 10^{-2} Hz, with an amplitude of 5 mV and a bias voltage of 1.53 V versus RHE. The electrochemically active surface area (ESCA) was assessed using the electrochemical double layer capacitance (C_{dl}) measured by cyclic voltammetry (CV) in the non-Faradaic region at scan rates of 20, 40, 60, 80, and 100 $mV \cdot s^{-1}$ within the potential range of 0.9 to 1 V vs. Hg/HgO. The ECSA was determined using the equation $ECSA = C_{dl}/Cs$, where Cs represents the specific capacitance of 0.04 $mF \cdot cm^{-2}$ in a 1 M KOH electrolyte. The catalyst's long-term durability was examined by chronoamperometry. The long-term durabilities of the catalysts were investigated by

chronoamperometry at 1.46 V vs. RHE.

S1.8. Theoretical calculation

All density functional theory (DFT) calculations were conducted within the CASTEP module of Materials Studio. The geometric optimization was performed using the Perdew-Burke-Ernzerhof (PBE) functional under the generalized gradient approximation (GGA). A plane-wave basis set with a kinetic energy cutoff of 400 eV was employed, and a vacuum space of 15 Å was implemented to minimize interactions between periodic images.

The intrinsic OER activity was quantified by determining the theoretical overpotential (η), which is governed by t the rate-determining step (RDS) possessing the maximum free energy change (ΔG_{max}) among the four-electron process. The calculation followed the established relationship: $\eta = (\Delta G_{max} / e) - 1.23$ V. The Gibbs free energy for each elementary step was formulated as $\Delta G = \Delta E + \Delta E_{ZPE} - T\Delta S$. Within this framework, ΔE denotes the change in electronic energy, while the zero-point energy correction, $E_{ZPE}=\frac{1}{2}\sum_i hvi$ (h: Planck constant; ν: vibrational frequencies).

S1.9 ICP-OES measurements

The concentrations of metal ions (Fe^{3+}, Ni^{2+}, Sn^{4+}) in the electrolyte after 50, 100, and 200 hours of stability testing were determined using an Inductively Coupled Plasma Optical Emission Spectrometer (ICP-OES). Standard solutions of Fe^{3+}, Ni^{2+}, and Sn^{4+} with concentration gradients of 0, 20, 40, 60, 80, and 100 μg/L (in 1% HNO3 solution) were used as calibration references. The electrolyte samples collected after stability tests of different durations were then analyzed as the test samples. The ICP-OES instrument was used to establish a calibration curve representing the relationship between emission intensity and concentration, based on measurements of the blank solution and the standard solutions. The data points were fitted to generate a trend line and its

corresponding equation, with a required coefficient of determination (R^2) of ≥0.999. The emission intensity at the specific characteristic wavelengths for each element in this test (Fe at 238.204 nm, Ni at 231.604 nm, Sn at 283.998 nm) was measured for the sample solutions, and their concentrations were precisely calculated using the trend line equation. The results indicate a highly linear correlation for Fe^{3+}, Ni^{2+}, and Sn^{4+} within the 0–100 μg/L concentration range. Based on the calculations, the concentrations of metal ions in the electrolyte after the 200-hour stability test were determined to be 0.037 μg/L for Fe^{3+}, 0.051 μg/L for Ni^{2+}, and 0.053 μg/L for Sn^{4+}. These extremely low leaching concentrations further confirm the excellent stability of the material.

S1.10 in situ Raman spectroscopy test

In situ Raman spectroscopy tests were conducted in a three-electrode system, using FeOOH/SnS_2/Ni_3S_2/NF as the working electrode, Hg/HgO as the reference electrode, and a carbon rod as the counter electrode. The measurements were performed in 1.0 M KOH electrolyte within a potential range from the open-circuit potential to 1.624 V vs. RHE. Raman signals were collected in the range of 100-1000 cm^{-1}, with a spectral integration time of 1 minute at each applied potential, enabling dynamic monitoring of structural changes in the catalyst during the OER process.

S1.11 Differential electrochemical mass spectroscopy (DEMS)measurements

The ^{18}O isotopic labeling DEMS measurements were conducted on an operando DEMS system, which consisted of a PFEIFFER QAS100 quadrupole mass spectrometer equipped with a turbopump (HIPACE 80, PFEIFFER) and an additional chamber connected to an electrochemical cell at ambient pressure. The generated gaseous oxygen products were directly transferred into the vacuum chamber for mass spectrometric analysis. For the electrochemical system, Hg/HgO and a platinum wire were used as the reference electrode and counter electrode, respectively. The catalytic

material SR-FeOOH/SnS_2/Ni_3S_2/NF served as the working electrode. First, five cycles were performed in a 1.0 M KOH/$H_2{}^{18}O$ electrolyte with a scan rate of 1 mV s^{-1} and a potential range from 0.92 V to 1.72 V vs. RHE to isotopically label the lattice oxygen in SR-FeOOH/SnS_2/Ni_3S_2/NF with ^{18}O. Then, the ^{18}O-labeled catalyst was rinsed with $H_2{}^{16}O$ water to remove residual $H_2{}^{18}O$. Finally, the aforementioned catalyst underwent six cycles in a 1.0 M KOH/$H_2{}^{16}O$ electrolyte. The mass spectrometer detected gaseous products such as $^{32}O_2$, $^{34}O_2$, and $^{36}O_2$ in real time.

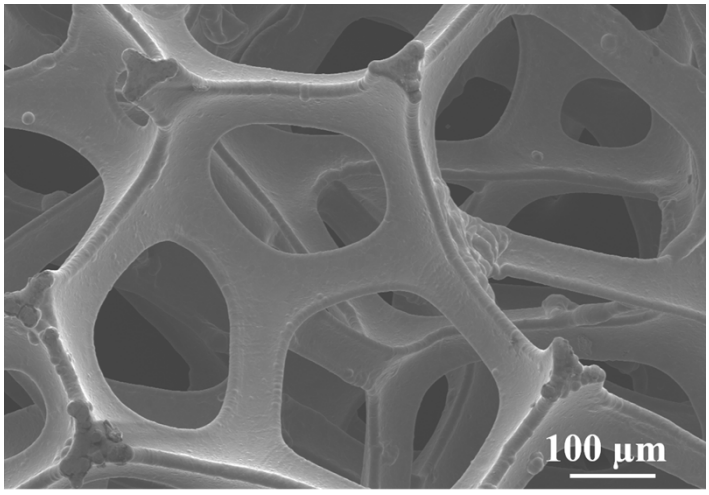

Fig. S1. The SEM of NF.

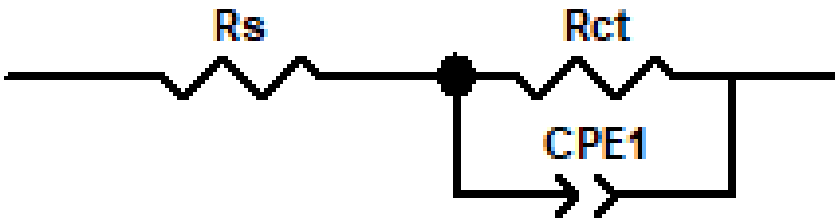

Fig. S2. The equivalent circuit model.

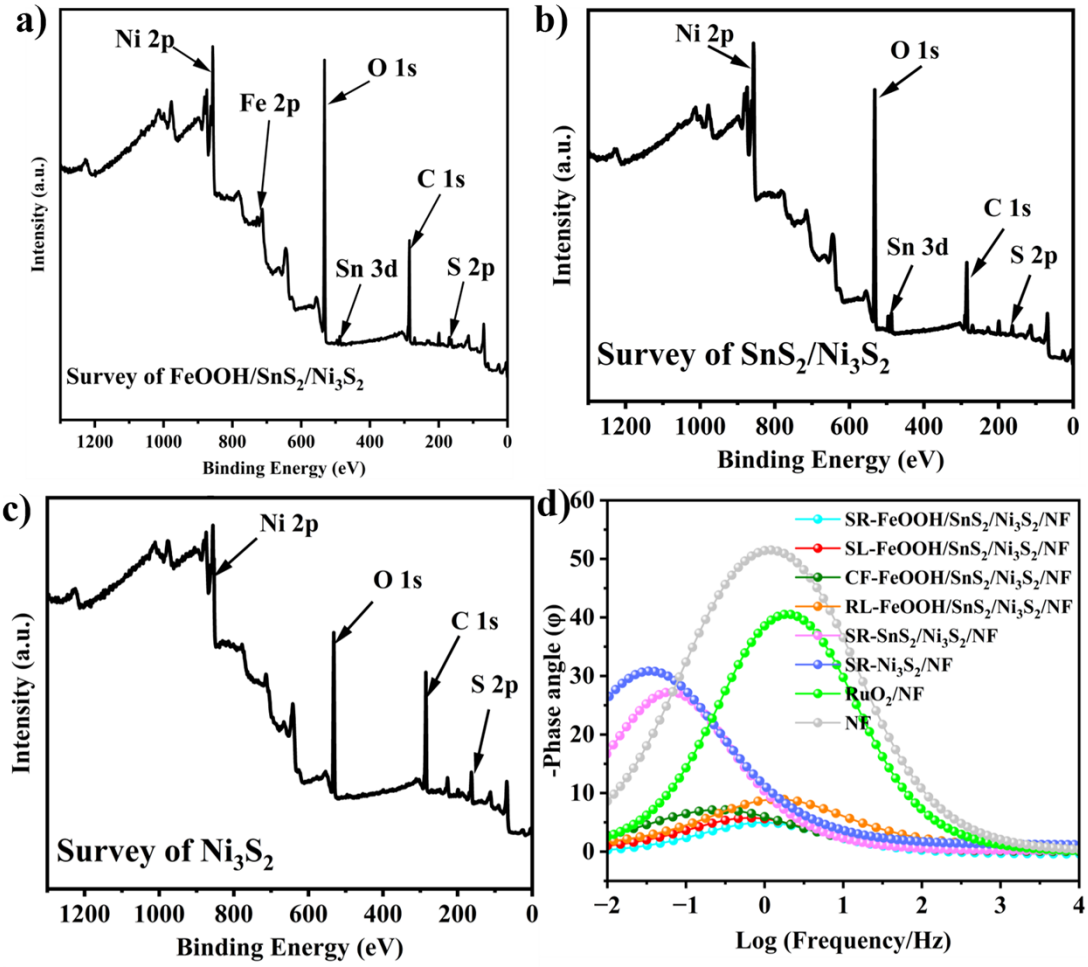

Fig. S3. XPS survey spectrum of (a) $FeOOH/SnS_2/Ni_3S_2$. (b) SnS_2/Ni_3S_2, and (c) Ni_3S_2. (d) Bode plots.

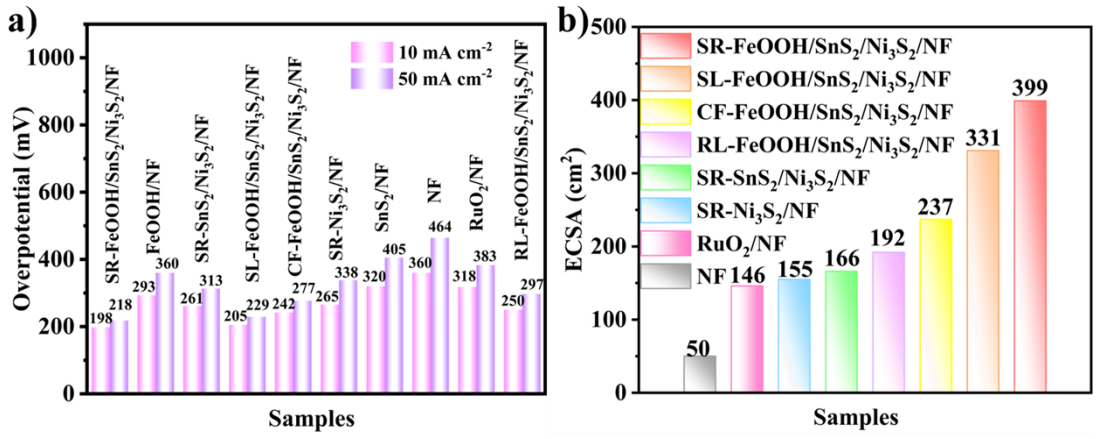

Fig. S4. (a) Overpotential histogram of different samples. (b) Calculation of ECSA values.

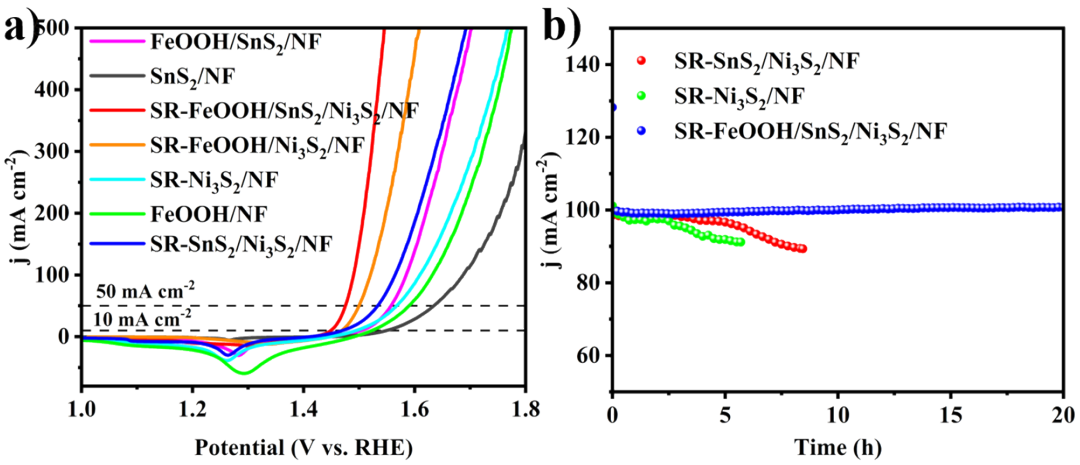

Fig. S5. (a) LSV polarization curve of different electrodes. (b) Stability tests of SR-FeOOH/SnS_2/Ni_3S_2, SR-SnS_2/Ni_3S_2, and SR-Ni_3S_2.

LSV polarization curve of different electrodes are tested to comprehensively and systematically explain the synergistic effects between different components (Fig. S5). It was found that the catalytic activity of two component catalysts (SR-FeOOH/Ni_3S_2/NF, SR-SnS_2/Ni_3S_2/NF, FeOOH/SnS_2/NF) is better than that of the single-component catalysts (SR-Ni_3S_2, SnS_2, FeOOH), and three component catalyst (SR-FeOOH/SnS_2/Ni_3S_2/NF) outperforms two component catalysts, indicating that the performance advantage of the SR-FeOOH/SnS_2/Ni_3S_2/NF stems from the synergistic effects between different components.

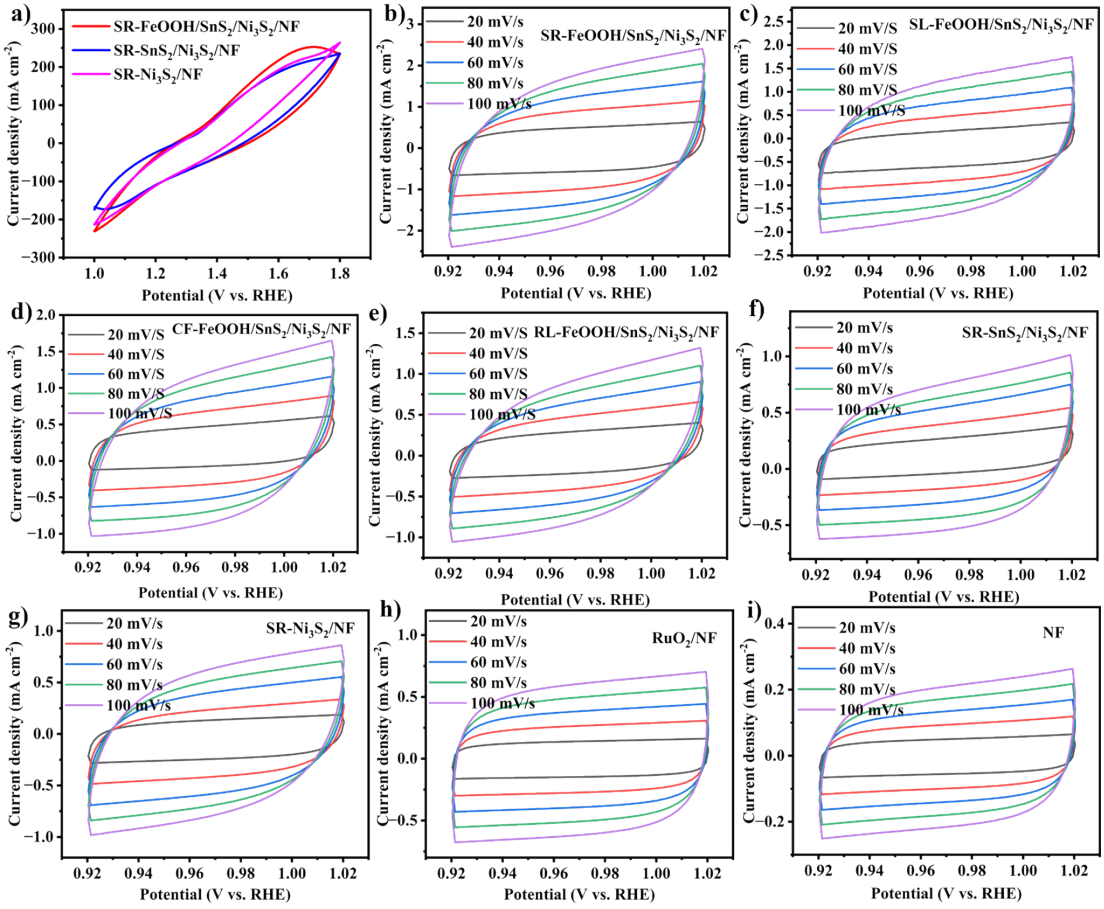

Fig. S6. (a) CV curves of SR-FeOOH/SnS_2/Ni_3S_2/NF, SR-SnS_2/Ni_3S_2/NF and SR-Ni_3S_2/NF in 1.0 M KOH with a scan rate of 50 mV s^{-1}. CV curves of the synthesized SR-FeOOH/SnS_2/Ni_3S_2/NF (b). SL-FeOOH/SnS_2/Ni_3S_2/NF (c). CF-FeOOH/SnS_2/Ni_3S_2/NF (d). RL-FeOOH/SnS_2/Ni_3S_2/NF (e). SR-SnS_2/Ni_3S_2/NF (f). SR-Ni_3S_2/NF (g). RuO_2/NF (h). and NF (i).

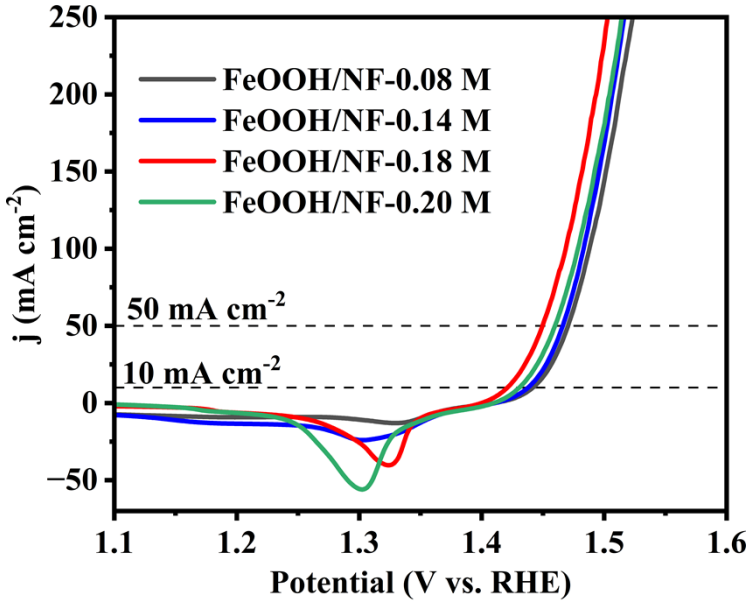

Fig. S7. FeOOH LSV with different loads on NF.

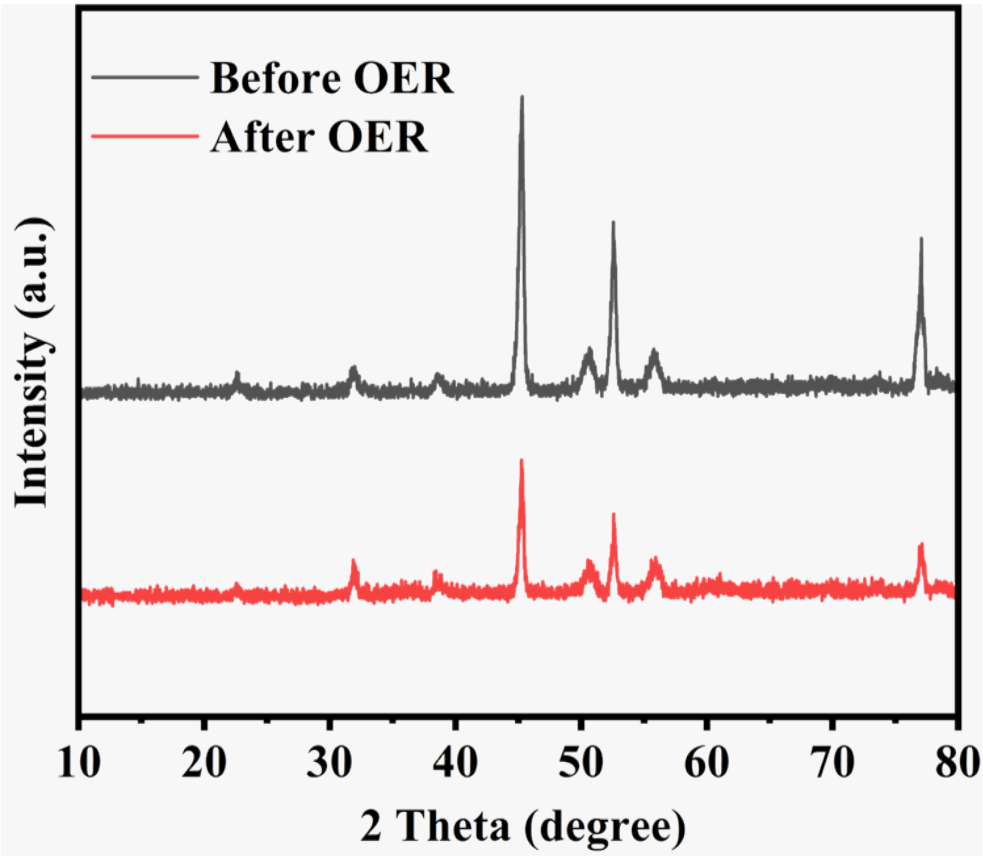

Fig. S8. The XRD of the FeOOH/SnS_2/Ni_3S_2/NF after OER stability test.

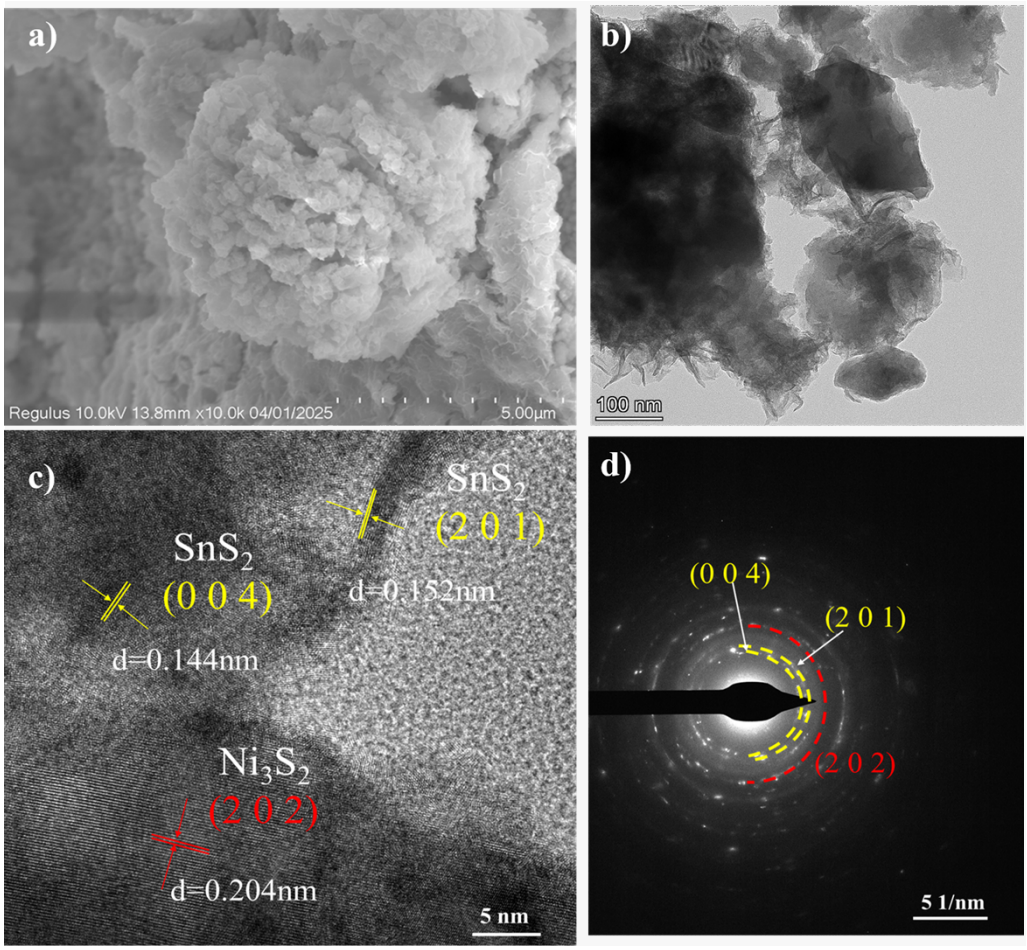

Fig. S9. The SEM image of (a) SR-FeOOH/SnS_2/Ni_3S_2/NF after OER stability test. The TEM (b) and HRTEM images (c) of SR-FeOOH/SnS_2/Ni_3S_2/NF after OER stability test. (d) SAED pattern of SR-FeOOH/SnS_2/Ni_3S_2/NF after OER stability test.

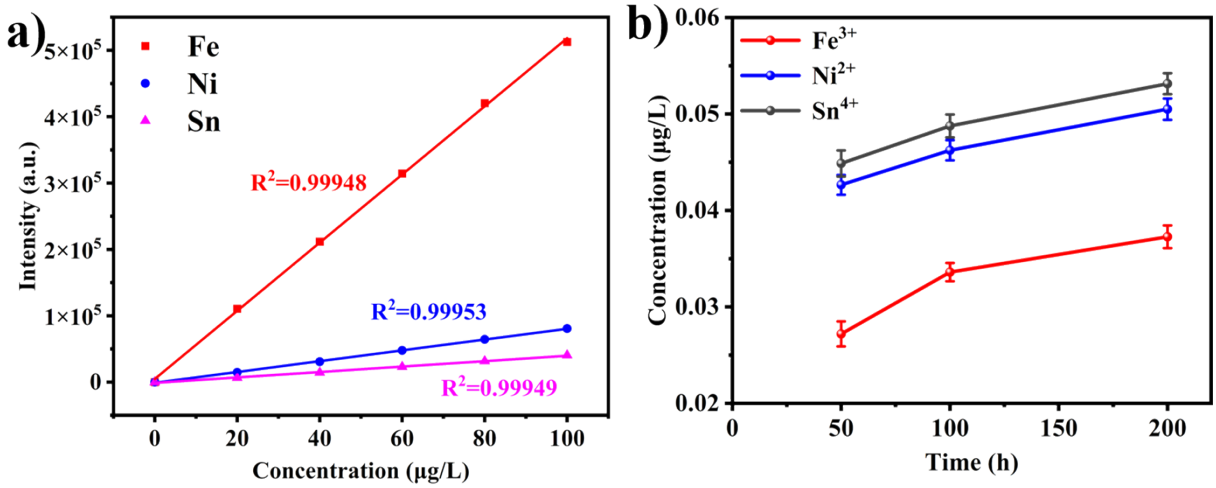

Fig. S10. (a) Linear fitting of Sn, Fe, and Ni to their concentrations in 1% HNO_3. (b) and (c) ICP-OES analysis results of metal ion dissolution in the electrolyte after stability tests of 50 h, 100 h and 200 h.

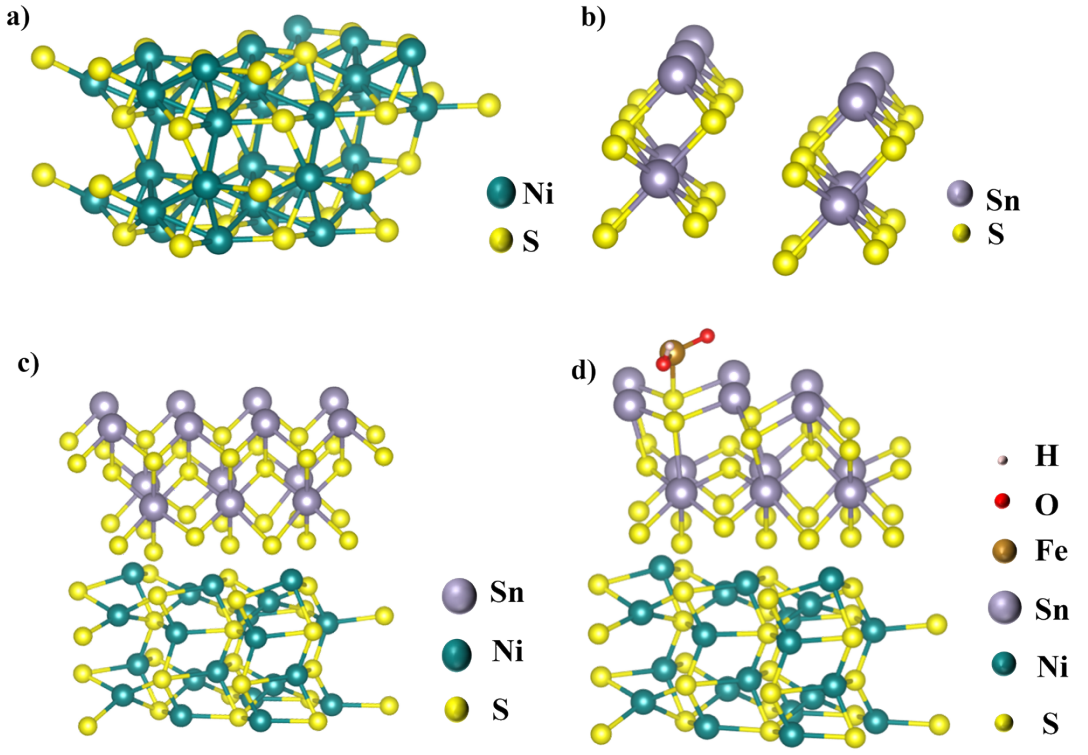

Fig. S11. Crystal structure of (a) Ni_3S_2 (202). (b) SnS_2 (100). (c) SnS_2/Ni_3S_2 and (d) $FeOOH/SnS_2/Ni_3S_2$.

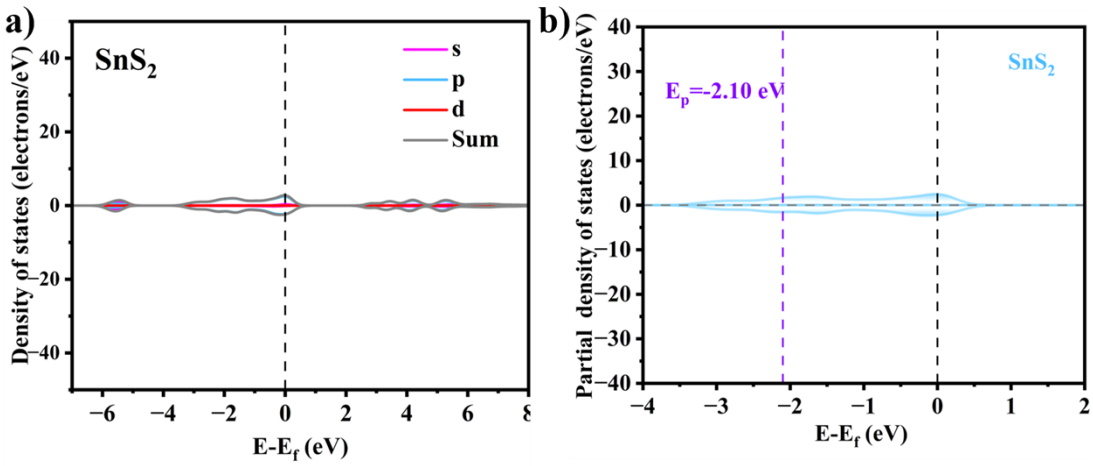

Fig. S12. DOS (a) and p-band center (b) of SnS_2.

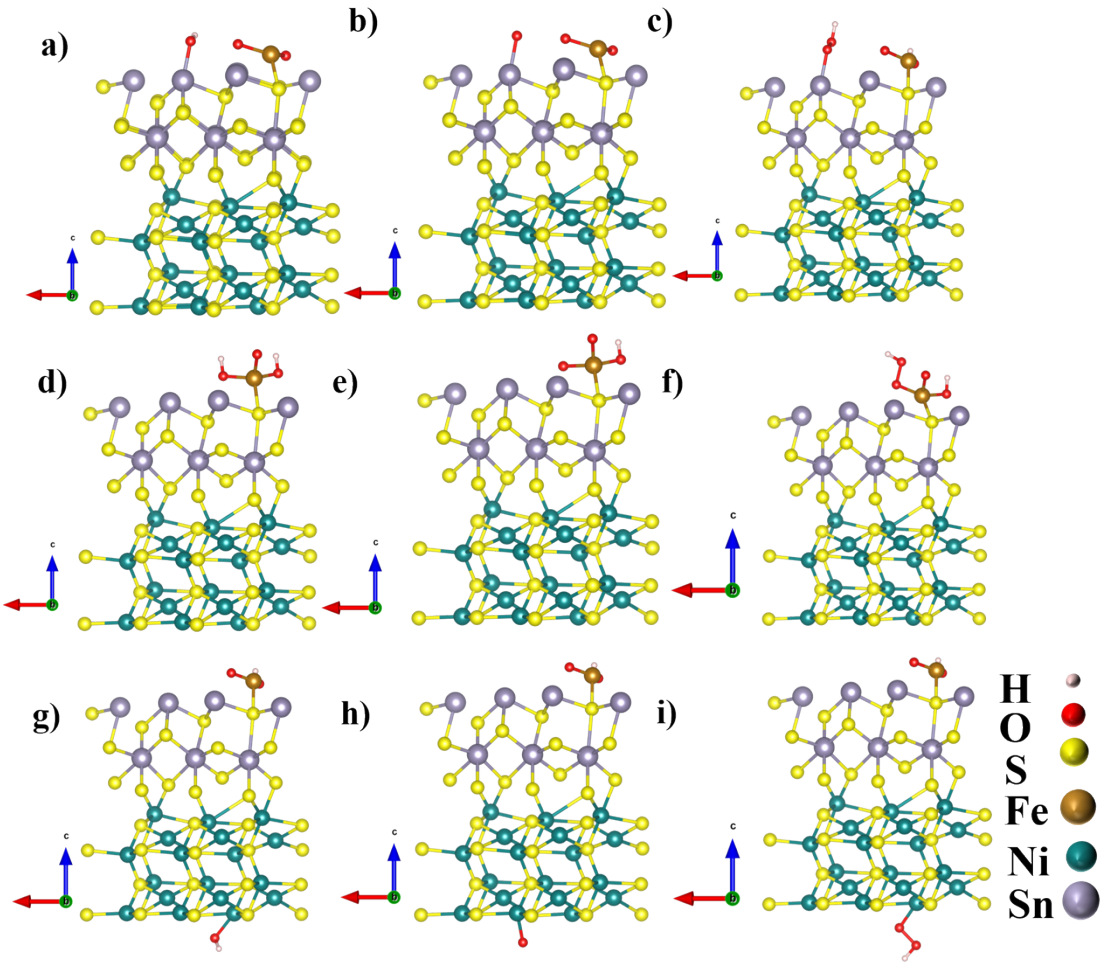

Fig. S13. Structural models of the key active sites in the FeOOH/SnS_2/Ni_3S_2 heterostructure. Sn-Site (a-c). Fe-Site (d-e) and Ni-Site (g-i) with the adsorption of OH, O and OOH.